Radial correlation effects on interconfigurational excitations at the end of the lanthanide series. A restricted active space second order perturbation study of Yb^{2+} and $SrCl_2$:Yb^{2+}.

Zoila Barandiarán[1,2] and Luis Seijo[1,2]

[1]*Departamento de Química, Universidad Autónoma de Madrid, 28049 Madrid, Spain*

[2]*Instituto Universitario de Ciencia de Materiales Nicolás Cabrera, Universidad Autónoma de Madrid, 28049 Madrid, Spain*

(Dated: January 21, 2013)

Abstract

At the end of the lanthanide series, $4f \rightarrow 5d$ and other interconfigurational transitions in which one electron is excited from a tight $4f$ orbital to a much more diffuse one, occur with a break of many f-f pairs, which make the electron correlation effects dominant. For instance, the large energy gap of 25000 cm^{-1} ($\sim$ 29500 cm^{-1} without spin-orbit coupling) above the $4f^{14}$ ground state of the $SrCl_2$:Yb^{2+} material is mostly due to electron correlation. In effect, a minimal multiconfigurational restricted active space (RASSCF) calculation that includes only the $4f^{14}$ ground and $4f^{13}5d$ and $4f^{13}6s$ open-shell excited configurations gives a very small gap (5400 cm^{-1}), whereas the correlation corrections to the $4f^{14} \rightarrow 4f^{13}5d(e_g)$ transition energies at the second order perturbation theory (RASPT2) level are very large: 35599$\pm$439 cm^{-1}, in average, for all excited states. These corrections are too large to be accurate at second order perturbation level. When a second f-shell is also included in the active space and single and double excitations to the $5d$, $6s$, and $5f$ shells are treated variationally, the (extended) RASSCF energy gap above the ground state and the electronic transitions increase by 22038$\pm$120 cm^{-1} and the RASPT2 correlation energy corrections become small (–721$\pm$571 cm^{-1}), as it is desirable for a second order perturbation. A comparative analysis of both RASPT2 results reveals that the lack of the second f-shell accounts for 12700 cm^{-1} of the 14223$\pm$80 cm^{-1} overestimation of interconfigurational transitions energies by the minimal RASPT2 calculation, which indicates an inaccurate calculation of the differential radial correlation between the $4f^{14}$ and $4f^{13}5d$ configurations by second order perturbation theory. In order to establish practical and accurate procedures for the calculation of $4f \rightarrow 5d$ and other interconfigurational transitions at the end of the lanthanide series, the above and other RASSCF/RASPT2 calculations on the ionization potential of Yb^{2+} in gas phase and in $SrCl_2$ have been benchmarked in this paper against coupled cluster (CCSD and CCSD(T)) calculations, and RASSCF/RASPT2 calculations on the absorption spectrum of $SrCl_2$:Yb^{2+} have been compared with experiment. The results support that variational calculation of SD $4f \rightarrow 5f$ excitations prior to RASPT2 calculations can be a realistic, accurate, and feasible choice to model radial correlation effects at the end of the lanthanide series.

I. INTRODUCTION

The electronic origin of the first excited state of Yb^{2+} in $SrCl_2$, where Yb^{2+} is in 8-fold cubic coordination of Cl^-, has been located 25000 cm^{-1} (3.1 eV) above the ground state by low temperature absorption and emission spectra.[1–3] First-principles electronic structure calculations have shown that this large energy gap is dominated by differential dynamic electron correlation, which amounts 30300 cm^{-1} (Ref. 4): Whereas the ground state, $1A_{1g}$, corresponds to the $4f^{14}$ configuration, the first excited state, $1E_u$, belongs to the $4f^{13}5d(e_g)$ one. Hence, electron correlation stabilization is much stronger in the ground state where the number of tight $4f$ pairs is larger. Opposite and much smaller contributions of non-dynamic electron correlation (+2000 cm^{-1}), together with spin-orbit coupling (–4500 cm^{-1}) lead to the theoretical prediction for the first $4f^{13}5d(e_g)$–$1E_u$ energy level: 27800 cm^{-1}, which overestimates the experimental value by 2800 cm^{-1} (11%).[4] Similar differential correlation effects were found in the whole $4f^{13}5d$ energy spectrum and a thourough comparison of electric dipole allowed theoretical and experimental transition energies showed a very good agreement once the whole theoretical spectrum was shifted by –3500 cm^{-1} to account for a constant interconfigurational error.[5] Given that the contribution of differential dynamic correlation amounts to ca. 94% of the spin-orbit free electronic transition(s) and that this contribution was calculated using multi-state second order perturbation over a particular complete active space (which includes only the relevant $4f$, $5d$, and $6s$ open shells), this constant error was interpreted as due to inaccuracies of the MS-CAS$(4f, 5d, 6s)$PT2 treatment at the end of the lanthanide series, which result in overcorrection of the ground state electron correlation. Hence, the need to investigate and improve the theoretical treatment of electron correlation at the end of the lanthanide series was a conclusion in Ref. 5 and became the central goal of the present work.

Although basically all lanthanide ions have technological and fundamental interest, the present theoretical issue is only expected to be significant for the heavier lanthanide ions (N>7), for which the ground state contains doubly occupied f orbitals and interconfigurational excitations reduce the number of doubly occupied orbitals. In the lighter lanthanides (N≤7), this effect is not important because the ground states do not contain doubly occupied orbitals. The atomic (lanthanide) contribution to the differential dynamic electron correlation between $4f^N$ and $4f^{N-1}5d$ states grows towards the right of the series and, at

the end of it, it becomes much larger than the molecular or ligand contribution, which is almost constant across the series.[6] Since the atomic lanthanide correlation increases the excitation (large in the $4f^N$ configuration) and the ligand correlation decreases it (large in the $4f^{N-1}5d$ configuration), the contributions of differential dynamic electron correlation to the $4f^N$–$4f^{N-1}5d$ transitions can be small and negative at the beginning and large and positive at the end of the series. This is shown in the trivalent lanthanide series Cs_2NaYCl_6:Ln^{3+} from Ce^{3+} (N=1) to Tb^{3+} (N=8) (Ref. 6) and in the divalent $SrCl_2$:Yb^{2+} case (N=14) (Ref. 5), where the contribution of differential dynamic correlation to the first $4f^N$–$4f^{N-1}5d$ transition varies from negative and small in Ce^{3+} (N=1) (–4800 cm^{-1}, 20% of the lowest spin-orbit free transition energy) and Pr^{3+} (N=2) (–2700 cm^{-1}, 7%), to negligible in Gd^{3+} (N=7) (1200 cm^{-1}, 0.02%), suddenly rising to positive and large in Tb^{3+} (N=8) (13000 cm^{-1}, 46%), and finally to dominant in Yb^{2+} (N=14) (30300 cm^{-1}, 94%).

Up to this point we have distinguished between non-dynamic and dynamic correlation contributions and have identified them with those portions of electron correlation included in the first, variational CASSCF step[7] and in the subsequent multi-state second order perturbation calculation,[8–11] respectively. However, in spite of the fact that near-degeneracy (widespread within the excited state manifods of lanthanide ions) is indeed included in the $4f, 5d, 6s$ CAS, the experience gathered over the last 30 years in first-series transition metal atoms and compounds suggests that the $4f$ radial correlation contributions to the total static correlation, which are lacking in the $4f, 5d, 6s$ CAS, and, therefore, have been calculated perturbationally, might be large at the end of the lanthanide series. This suggests the variational treatment of the $4f$ radial correlations is a necessary theoretical improvement for the heavier lanthanide defects.

Regarding radial correlations in open-shells, as early as 1977 and 1980, Froese-Fischer[12] and Dunning *et al.*[13] pointed out the inadequacy of the "equivalence" restriction of the Hartree-Fock method to properly describe the electronic structure of states of the $4s^13d^{N+1}$ and $3d^{N+2}$ configurations and their energy relative to the $4s^23d^N$ states for Ti and Ni (Ref. 13), and Cu (Ref. 12). They showed that, as one or two electrons are added to the $3d$ shell, one ($3d'$) or two ($3d'$, $3d''$) orbitals are "functionally inequivalent" and more diffuse than the rest of $3d$ orbitals, so that the proper orbital configurations of these states are rather $4s^13d^N3d'$ and $3d^N3d'3d''$. The authors showed the significance of this correlation contributions by performing multiconfigurational Hartree-Fock calculations using an extra

$4s3d^N4d$ configuration involving a second d-shell. Andersson and Roos faced the same basic type of radial correlation interaction in the context of a CASPT2 study of excitation energies of the Ni atom,[9] where they showed the need to include a second d-shell in the CAS space. More recently, Pierloot and collaborators have investigated further the need to include double d-shells in the CASSCF (and RASSCF, see below) space in the context of large basis set CASPT2 (and RASPT2) calculations on transition metals and their compounds, and have concluded that the double-shell effect is more important (a) for the heavier transition metal ions (d^N; N>5) than for the lighter, (b) for transition energies involving a change of the nd occupation, and (c) for first-row than for second- and third-row transition metals.[14–17]

It is, therefore, the purpose of this paper to investigate the effects of radial correlation in the $4f$ shell in the spectroscopy of lanthanide defects in ionic solids at the end of the lanthanide series, adapting the knowledge and methods developed so far for transition metal compounds to the specific features of lanthanides.

We must bear in mind that the high complexity of the excited manifolds of lanthanide ions in solids will force us to face many shells and many configurations at the same time. The spectroscopy of lanthanide ions in solids is very complex, yet two types of electronic transitions contain most of the effort on basic and applied spectroscopic research: the $4f^N - 4f^N$ and $4f^N - 4f^{N-1}5d^1$ spectroscopies. The intrashell $f - f$ transitions should not be significantly affected by differential radial correlation, therefore, we focus on the latter in this paper, taking the most demanding $N = 14$ ($4f^{14}$) Yb^{2+} ion as the case study. $4f^{N-1}5d^1 \rightarrow 4f^N$ luminescence is the core of lanthanide based solid-state-lighting, scintillators, and other devices; however, the efficiency of the $4f^{N-1}5d$ emissions may be seriously compromised by impurity-trapped excitons which may occur above, among, or below them in energy, depending on the particular impurity-host combination. This means that an *ab initio* study cannot disregard them. In previous works we have described the electronic structure of impurity-trapped excitons using wavefunction-based quantum chemical methods and language[4,18] as excited states of the $4f^{N-1}\phi_{ITE}$ configuration, not so localized as the regular impurity states ($4f^N$, $4f^{N-1}5d^1$, $4f^{N-1}6s^1$), but still bound to the impurity, which pour significant electron density beyond first neighbours, to the nearest interstices or cations.[4,18,19] Should this type of excited state occur among or below the $4f^{N-1}5d^1$ manifolds, their explicit calculation is unavoidable. In these cases, apart from cluster and basis set extensions, a minimal meaningful orbital active space must contain the impurity $4f$, $5d$, $6s$, and the impurity-trapped exciton

ϕ_{ITE} open shells. Furthermore, depending on the material (impurity-host combination), the number of ITE shells can be so large as to outnumber the impurity open shells.[19] It is important to bare all of this in mind if realistic, accurate, and feasible recipes for including radial correlation involving an additional $5f$ shell are to be designed.

It is clear that a complete active space of N electrons in $4f$, $5d$, $6s$, and $5f$ orbitals (N electrons in 20 orbitals) is not a feasible alternative; this is also true when the impurity site symmetry is high. Obviously, this is still worse if ITE's are to be included in the active space. A much more versatile tool, capable to focus the multireference space on the lanthanide open-shell structure demands, is the restricted active space followed by multi-state second order perturbation theory method (MS-RASPT2) proposed by Malmqvist *et al.*[16] For these reasons, we have used this method throughout this work. We have excluded the ϕ_{ITE} shells from the active space because we focus on the lowest energy excited manifold of Yb^{2+}-doped $SrCl_2$, which is entirely below the first $4f^{N-1}\phi_{ITE}$ state.

We have studied different choices of active space and excitation order in RASPT2 calculations of the Yb^{2+} free ion ionization potential, in the first place. This allows benchmarking the RASPT2 results *vs.* single-determinant based CCSD(T) calculations. Besides, the known relationship between $4f^N \rightarrow 4f^{N-1}$ ionization potentials and $4f^N \rightarrow 4f^{N-1}5d$ electronic transitions in the lanthanide series makes it reasonable to use it as a simpler model to decide upon for the new standard of calculations for the ion embedded in a crystal. Furthermore, the study of the ionization is very meaningful here where the effects of radial correlation in the $4f$ shell are on focus. We have also studied the ionization of Yb^{2+} embedded in the $SrCl_2$ crystal and the lowest $4f^N \rightarrow 4f^{N-1}5d$ transitions using the embedded cluster approximation. In both cases the RASPT2 calculations were done using the new standard decided upon in the free ion, and CCSD(T) and previous theoretical-experimental results were used in benchmarking. Two alternative spin-orbit free Hamiltonians have been used in the free ion: the valence only *ab initio* core model potential method (AIMP)[20] with open-shell Hartree-Fock valence basis sets and the all electron Douglas-Kroll-Hess method (AE-DKH)[21,22] with relativistic atomic natural orbital basis sets (ANO-RCC).[23] Only the latter has been used in the embedded cluster calculations.

The methodological details are presented in Sec. II and the results are presented and discussed in Sec. III. The conclusions on the role of $4f$ radial correlations and the proposal of recipes for efficient and feasible calculations of excited manifolds at the end of the lanthanide

series are presented in Sec. IV.

II. METHODS AND DETAILS OF THE CALCULATIONS

Most of the calculations presented in this paper have a first step where multiconfigurational self-consistent field wavefunctions and energies are calculated using complete and/or restricted active spaces (CASSCF[7] and/or RASSCF[24,25]). We will describe the particular choices of active space following the usual convention for the classification of orbitals into INACTIVE, RAS1, RAS2, RAS3, and EXTERNAL subsets: All orbitals have occupation number 2 in the INACTIVE subset and 0 in the EXTERNAL subset, and a number of so-called active electrons are distributed among the active orbitals, which are grouped in three subsets with possible occupation number 0, 1, or 2, and the following restrictions, besides those of leading to a multielectronic wavefunction of a given total spin and spatial symmetry: orbitals in RAS1 are initially fully occupied and a maximum number of holes is allowed (nh); there are no additional restrictions to the occupation of the orbitals in RAS2; orbitals in RAS3 are initially empty and a maximum number of electrons is allowed (ne). Consequently, we will refer to the composition of the three subsets forming the restricted active space as follows: RAS(orbitals-nh/orbitals$'$/orbitals$''$-ne) or similar. The number of active electrons is 14 for Yb^{2+} and 13 for Yb^{3+} in gas phase and in the solid. The orbitals are optimized in a state average in all cases except in single reference states. The state average includes all states with main $4f^{13}5d^1$ and $4f^{13}6s^1$ configurational character of a given total spin and D_{2h} symmetry block in the case of Yb^{2+}-doped $SrCl_2$. (Note that we refer to molecular orbitals and leading configurations by their main lanthanide orbital character. Although approximate, this practice is appropriate in lanthanide-ion doped ionic crystals.) As indicated, some atomic calculations have been done using D_{2h} symmetry for convenience; some others use C_i symmetry. These alternatives are both acceptable since the results differ in the order of 10^1 cm^{-1}, which does not affect the discussions nor the conclusions. The solid state calculations are done using D_{2h} symmetry with restrictions to the orbital rotations to enforce actual O_h site symmetry.

In all but the single reference $4f^{14}$ and $4f^{13}$ cases, the state-average CAS/RASSCF states of lanthanide ions in gas phase and in solids are known to interact at second order perturbation level. Therefore, dynamic correlation must be computed using the multi-state

multiconfigurational second order perturbation theory (MS-CASPT2[8–11] or MS-RASPT2,[16] respectively), which is the standard choice in this work. Hence, the usual MS- prefix will be omitted in the text, tables, and figures. In all cases 22 (Yb^{2+}) or 21 (Yb^{3+}) valence electrons have been correlated corresponding to the Yb $5s$, $5p$ closed-shells and $4f$, $5d$, $6s$ open-shells. In the embedded cluster calculations, 64 additional valence electrons corresponding to the $3s$ and $3p$ valence shells of the eight first neighbour chlorines are also correlated. We will refer to this choice as L64M22 or L64M21. The standard IPEA value (0.25 au) has been used in the calculation of the electronic transitions of Yb^{2+}-doped $SrCl_2$; it has been set to 0 otherwise. This parameter has been introduced in Ref. 26 as a simple way to correct for systematic underestimations of CASPT2 transition energies from closed-shell ground states to open-shell excited states, although it is also recommended as default option in other cases. The IPEA value should be comparable to IP – EA, the difference between the IP and EA energies (EA = electron affinity, EA),[26] which, considering J-weighted averages, are 0.2, 0.2, and 0.5 au for Yb, Yb^+, and Yb^{2+} in gas phase, respectively.[27–29] The effect of this parameter is an increase of the electronic transition energies calculated in $SrCl_2$:Yb^{2+} by about 800 cm^{-1}.

Two relativistic Hamiltonians have been used excluding their spin-dependent terms. Most calculations of the ionization potential of Yb^{2+} in gas phase have been done using the spin-orbit free Wood-Boring *ab initio* model potential (AIMP) method,[20] using the [Kr] core AIMP[30] and corresponding valence basis set $(14s10p10d8f)$,[31] supplemented with three g-type functions that give maximum radial overlap with the $4f$ atomic orbital, contracted as $[6s5p6d4f1g]$. Second order all electron Douglas-Kroll-Hess (AE DKH)[21,22] calculations have been done to compute the ionization potential of Yb^{2+} in gas phase and in $SrCl_2$, and the lowest electronic excited states of $SrCl_2$:Yb^{2+}. The all electron relativistic atomic natural orbital (ANO-RCC) basis sets for Yb $(25s22p15d11f4g2h)[9s8p5d4f3g2h]$ and Cl$(17s12p5d4f2g)[6s5p3d]$ were used.[23] Extensions to these bases were considered in the solid state calculations, as explained below.

The AIMP and AE DKH hamiltonians have also been used to perform iterative Coupled Cluster singles and doubles (CCSD(T)) calculations for the single-determinant ground states of Yb^{2+} and Yb^{3+} in gas phase and in the $SrCl_2$ solid using D_{2h} symmetry (only the single determinant $^2A_{2u}$ component of the $4f^{13}$ configuration was calculated). For the noniterative triples contribution (CCSD(T)), the method of Raghavachari *et al.*[32] has been used for

the closed-shell Yb^{2+} ground state whereas that of Watts *et al.*[33] has been used for the single determinant open-shell Yb^{3+} ground state. Only the amplitudes of double excitations from inactive to external orbitals have been spin-adapted.[34,35] In all cases, the number of electrons correlated in these calculations is the same as in the CAS/RASPT2 calculations being compared to the CCSD(T) results.

Yb^{2+} occupies Sr^{2+} sites at (0,0,0) in the ionic fluorite-like $SrCl_2$ crystal. Its site symmetry is O_h and it is surrounded by 8 first-neighbour Cl^- at (x,x,x) (x=1/4 in the undistorted lattice and $x = d(\mathrm{Yb}-\mathrm{Cl})/\sqrt{3}$ in the doped material), 12 second-neighbour Sr^{2+} at (1/2,1/2,0), and 6 interstitial sites at (1/2,0,0).[36] All of these sites define a volume where the wavefunctions of the impurity states and impurity-trapped excitons are localized.[4] Consequently, the embedded cluster approximation can be used. The defect cluster defined in this work contains up to second neighbours: $(YbCl_8Sr_{12})^{18+}$. Its electronic structure is calculated using the methods referred above with extensions to the Yb and Cl basis sets which involve Sr and interstitial basis functions as mentioned below. The effects of the remaining lattice ions on the cluster electronic structure are incorporated into the embedded-cluster Hamiltonian by using the AIMP embedded-cluster method,[37,38] which ensures that classic and quantum mechanical interactions are considered. The embedding potentials have been obtained in Ref. 4 to represent the Sr^{2+} and Cl^- ions located at their cubic crystal structure sites (Group 225, $Fm\bar{3}m$, $a_0 = 6.9744$ Å[36]); the potentials were obtained by performing self-consistent embedded Sr^{2+} and Cl^- ions calculations at the Hartree-Fock level on the perfect host crystal as described in Ref. 38. All ions located at a distance smaller or equal to 14 Å from the $YbCl_8$ sites contribute to the cluster Hamiltonian as full AIMPs. An additional set of point charges is used to ensure that the Ewald potential is reproduced within the cluster volume. These charges are obtained following the method of Lepetit *et al.*[39]

The program MOLCAS has been used for all calculations.[40] All AIMP data (for embedding and/or for cores) and valence basis sets can be found in Ref. 41.

III. RESULTS AND DISCUSSION

A. Yb^{2+} in gas phase.

The purpose of the work reported in this Section is to find out what type of RASPT2 calculations yields comparable values of the ionization potential (IP) of Yb^{2+} to those obtained using the CCSD(T) method. This investigation reveals that the inclusion of a second f-shell in the restricted active space of RASPT2 calculations is crucial to accomplish near CCSD(T) accuracy. The conclusions of this Section are a guide to design the RASPT2 calculations of Yb^{2+} in the $SrCl_2$ solid presented in Secs. III B and III C.

We have calculated the IP using different restricted active spaces including and not including a second f-shell. These calculations have been done using the [Kr] core AIMP and $[6s5p6d4f1g]$ valence basis set for Yb described in Sec. II. The results are presented in Table I. The first two active spaces listed in the table (calculations 1 and 2) are the minimal, single-determinant one and the $[4f5d6s]^{14}$ complete active space. The latter is the standard CAS used in lanthanide ions doped in solids and includes the most relevant open shells of the ion.[42] (Note the size of the configurational space generated by this CAS even though it only includes one f-shell and D_{2h} symmetry has been used.) Following these, a number of restricted active spaces are presented which do not include double sets of f orbitals (calculations 3 to 6). They show that the CAS($4f5d6s$)PT2 result can be approached at the RASPT2 level with much smaller RAS, even when only singles and doubles (SD) excitations to the $5d6s$ shells are allowed. All of these results are 13700 cm^{-1} (7%) too high compared with the CCSD(T) benchmark and they show the drawbacks of these RAS+PT2 combinations.

In effect, when a second f-shell is included in the same restricted active spaces (calculations 7-9 and 11-13), the correlation correction drops to values much closer to the CCSD(T) result and the deviations of the RASPT2 vs. CCSD(T) decrease from 13700 cm^{-1} (7%) to $\pm$2000 cm^{-1} (less than 1%). In particular, SD excitations to the second f-shell decrease the IP by 13100 cm^{-1} (from calc. 1 to calc. 7), whereas SD excitations to the $5d$ shell increase it by 1350 cm^{-1} (from calc. 7 to calc. 8), and the effects of SD excitations to other higher unoccupied shells are negligible. The comparison of the RASPT2 values where SD or SDTQ excitations are allowed reveals that improvement of the triples calculation results

in an increase of the IP. This trend agrees with that shown by the coupled-cluster method calculations CCSD *vs*. CCSD(T). The number of configurations generated (adapted to D_{2h} symmetry) going from SD to SDTQ also grows by one or two orders of magnitude.

Comparison of the CCSD(T) and RASPT2 of near CCSD(T) accuracy (calculations 7 to 14) with the spin-orbit averaged experimental value of the IP of Yb^{2+} reveals discrepancies of –6000 to –10000 cm^{-1} (3–5%). Here we can recall that the importance of high angular momentum basis functions in the calculation of the third and fourth IP of lanthanides was stressed by Cao and Dolg in a basis set limit extrapolation of ACPF and CCSD(T) results.[43] The conclusions of their work suggest that the underestimations we have just mentioned could be ascribable to basis set limitations rather than to the AIMP (valence-only) approximation. Hence, since the double f-shell and valence basis set improvement effects could have opposite signs (cf. Table I and Ref. 43), which could result in cancellations of errors, and better agreements with experiment than those shown in Table I are desirable, the valence basis set quality has been examined, paying particular attention to the high angular momentum basis functions, as suggested by the results of Ref. 43. The work reported in Table II focus on these aspects.

The results of Table II show that when the $(3g)/[1g]$ contracted function used in the calculations of Table I, which was obtained from maximum radial overlap with the $4f$ atomic orbital, is split, all the IP values strongly increase, as expected from the conclusions of Ref. 43. Furthermore, when these g functions are substituted by the g-type atomic natural orbitals of the ANO-RCC all-electron basis set of Roos *et al.*,[23] the poor quality of the former becomes more clear and the valence-only AIMP and all-electron DKH results using the same type and number of g functions become very close. This is so for the two types of RASPT2 calculations performed, with discrepancies of the order of 1300 cm^{-1} (less than 1%). In this way, when the ANO-RCC g-type functions are used and SD excitations are allowed to the $5d5f6s$ shells, the RASPT2 results using both Hamiltonians come very close to the experimental value and the underestimations are reduced to –2000 cm^{-1} (AIMP) and –1000 cm^{-1} (AE DKH) for the $3g$ bases. This result is further improved when 2 h-type functions are used, as shown by the AE DKH results.

It should be noted that the effect of including SD excitations to the $5d5f6s$ shells in the RAS is very insensitive to the quality of the g set and to the Hamiltonian used, as shown in the column labeled "3 – 2" of Table II. A quite constant value of –12000 cm^{-1} is obtained.

This, together with the effect of SD excitations to the $5d$ shell (+1300 cm^{-1}) and to the $6s$ shell (negligible) previously commented (Table I), results in a net effect of the second f-shell of about –13300 cm^{-1}, very close to that shown in Table I. Finally, an increase of multiconfigurational space size and of the IP values of Table II should be expected if higher excitations were allowed in the RAS, as discussed above. This could increase the AE DKH $[9s8p5d4f3g2h]$ value of the IP, turning its discrepancy with experiment from -182 cm^{-1} to about 2600 cm^{-1}.

B. Yb^{2+}-doped $SrCl_2$. Ionization potential.

In this Section we present the results of spin-orbit free AE DKH RASPT2 calculations of the IP of Yb^{2+}-doped $SrCl_2$ using two types of RAS including and not including a double f-shell, in order to show the effects of improving $4f$-shell radial correlation. They are compared with single-determinant based CCSD(T) calculations, something that cannot be done with the electronic spectra, where the multireference nature of the electronic excited states cannot be avoided. Hence the interest of this comparison, which should serve to further support the choice of RAS. Besides, since the IP can help to select practical, accurate molecular basis sets for the calculation of the electronic spectra because of the the characteristics of the target impurity-states and impurity-trapped exciton (preionized) states mentioned above, here we will also study the choice of molecular basis set, starting by a selection of the Yb and Cl bases, to continue with extensions that incorporate basis functions at the second neighbour Sr and interstices.

Firstly, truncations of the quadruple-zeta plus polarization ANO-RCC basis sets of Yb and Cl have been considered while calculating the vertical IP at a given Yb–Cl distance using two different restricted active spaces. The results are presented in Table III. They indicate that the choice Yb $[9s8p5d4f3g2h]$ and Cl$[6s5p3d]$, which assumes the removal of the Cl $4f$ functions, is acceptable (truncation errors smaller than 100 cm^{-1} for the spaces used). Lowering the number of Cl d functions or removing the Yb h functions give errors of the order or larger than 500 cm^{-1}. Also, the valence-only AIMP results with the Yb$[6s5p6d4f1g]$ and Cl$[3s4p1d]$ valence basis sets (commonly used in regular CASSCF/CASPT2 calculations on lanthanide ions in ionic hosts) are included in Table III. They show errors of almost -9000 cm^{-1} in the two RAS. These errors should be attributed to the previously discussed

deficiencies in the high angular momentum components of the Yb AIMP valence basis set, because the corresponding results on the IP of free-Yb^{2+} (Sec. III A, Table II) give very similar errors: -9087 and -8642 cm^{-1} with the two RAS (209381 vs. 218468 cm^{-1} and 197623 vs. 206265 cm^{-1}). Finally, the deviations of the RASPT2 from the CCSD(T) results are analogous here and in the free-ion: 14135 vs. 13401 cm^{-1} with the small RAS and 2120 vs. 1198 cm^{-1} with the extended RAS. SD excitations to the $5d5f$ shells make the RASPT2 results approach the CCSD(T) ones by 12000 cm^{-1} in both cases. This improvement is, again, quite independent of the basis set used.

In embedded cluster calculations, the local structure of the defect cluster not only depends on the basis sets of the cluster atoms, but also on the basis sets used for neighboring atoms, because of the strong orthogonality conditions[44] that must be fulfiled between the cluster wavefunctions and the frozen ion wavefunctions of the embedding, represented by the AIMP embedding potentials. For this reason, the outermost atomic orbitals of the frozen embedding ions are customarily used in the cluster molecular basis set, which avoids artificial cluster bond length shrinkage.[38] In addition to this, otherwise empty orbitals of the next neighbour cations and functions at interstices (Int) have been found to be necessary for a balanced representation of impurity states and impurity-trapped excitons.[4,18] Consequently, the cluster definition and the Yb and Cl basis sets chosen above have been extended as indicated in Table IV, where the effects of such extensions on the Yb-Cl bond lengths, totally symmetric vibrational frequency of the $YbCl_8$ moiety, and adiabatic IP are presented.

When the cluster is extended to include the Sr^{2+} second neighbours and Sr and Int basis functions of Ref. 4 are used (Table IV, B *vs.* A), expected (but large) bond length expansions are observed ($^1A_{1g}$: +0.08 Å; $^2A_{2u}$: +0.06 Å), together with significant increases of the adiabatic IP (+10000 cm^{-1}). These effects are very similar when the RAS($4f$) and RAS($4f/5d5f$-$2e$) are used and also at the RASSCF or RASPT2 levels of calculation. Given that the Sr and Int extensions were obtained in Ref. 4 in valence-only AIMP calculations rather than in AE DKH calculations, and that their impact on the bond lengths and IP is large, convergence of the results with the Sr and Int extensions has been checked in this work using a more demanding procedure than that of Ref. 4. Details of this study are given in Ref. 45. As a result, a larger, reasonably converged basis set was found whose results are presented in Table IV C and in Sec. III C. The recipe for constructing the first neighbour Sr^{2+} cations and interstitial bases is as follows: The outermost orbitals of the

frozen embedded cation orbitals must be used (to fulfil cluster-embedding orthogonality) together with the Gaussian primitives with significant coefficients in the outer lobes of the empty cation orbitals, forming, altogether, at least a QZ basis set. In particular, the use of p-type Gaussian function of the cations first neighbors to the cluster (second neighbors to Yb) has turned out to have considerable impact on the bond lengths of impurity states and the IP. These functions have also been found to contribute significantly to the description of low-energy impurity-trapped excitons (ITE) of a similar system: BaF_2:Pr^{2+}, where ITEs occur below the $4f^15d^1$ manifolds; they luminesce and their excited (preionized) electron is attracted by the twelve (1/2,1/2,0) Ba^{2+} sites, where it localizes.[19] Interstice basis functions are also needed and can be optimized for the higher energy ITEs found in $SrCl_2$:Yb^{2+} (Ref. 4) and in BaF_2:Pr^{2+} (Ref. 19).

Comparisons of the minimal RAS($4f$)PT2 and the RAS($4f/5d5f$-$2e$)PT2 IP values with CCSD(T) results performed using the smallest of the two extended basis sets[4] (Table IV, B) give the same information as that obtained in the Yb^{2+} free ion in Table II: the large discrepancy of the minimal RASPT2 results: 13400 (Yb^{2+}) and 12900 (SrCl2:Yb^{2+}), are reduced to 1200 (Yb^{2+}) and 1200 (SrCl2:Yb^{2+}). The -12000 cm^{-1} effect on the IP of including the SD excitations to the $5d5f$ shells is maintained with the extensions of the cluster basis sets and it is quite independent of the basis set used (Table IV A–C).

Finally, the RASPT2 bond lengths appear to be too short compared with the CCSD(T) values by 0.02–0.03 Å. Improvements in the ligand correlation treatment on the line of incorporating ligand orbitals into the RAS might improve this result; however, this study is beyond the scope of this work. Note that bond length offsets between ground and excited states, rather than absolute bond length values, determine the characteristics of the absorption/emission band envelopes. A hint of the quality of such offsets can be obtained comparing the RASPT2 and CCSD(T) results: –0.162 Å in RAS($4f$)PT2), –0.165 Å in RAS($4f/5d5f$-$2e$)PT2 and –0.168 Å in CCSD(T). The second f-shell effect goes in the right direction.

C. Yb^{2+}-doped $SrCl_2$. $4f^{13}5d(e_g)$ excited states.

The results of multi-state RASPT2 all electron DKH calculations of the energy curves and spectroscopic constants of the lowest excited state manifold, $4f^{13}5d(e_g)$, are presented

in Fig. 1 (RASSCF and RASPT2 results) and Table V (RASPT2 results and PT2 contributions) and are discussed next. Taking as a guide the results of previous sections, the Yb[9s8p5d4f3g2h], Cl[6s5p3d], Sr[5s4p], Int[4s] basis set was used (Table IV C, Ref. 45), together with two different restricted active spaces.

We will first discuss the electronic transitions and analyze the equilibrium bond lengths and vibrational frequencies later.

The minimal active space capable of producing the $4f^{14}$ *gerade* ground state and all the $4f^{13}5d$ and $4f^{13}6s$ *ungerade* excited states of Yb^{2+} in $SrCl_2$, of which the $4f^{13}5d(e_g)$ is the lowest excited manifold, as well as the $4f^{13}$ $^2A_{2u}$ state of Yb^{3+}, is the RAS($4f$/5d6s-1e), in which a 5d and 6s orbitals are allowed to have up to one electron. This space generates a handful of configuration state functions. The RASSCF results show virtually no energy gap between the ground state and the $4f^{13}5d(e_g)$ manifold (Fig. 1). Consequently, the correlation energy corrections calculated at the subsequent RASPT2 step are very large, an average of 35599±439 cm^{-1}; as a matter of fact, too large to be calculated as a perturbation.

When additional SD excitations to the open 5d and 6s shells and to the second f-shell (5f) are allowed on top of the RAS($4f$/5d6s-1e), which is accomplished with the RAS($4f$-3h/5d6s/5f-2e), dramatic changes are observed, which are mainly associated with the second f-shell effect. In effect, the RASSCF results, which now correspond to $\sim 10^4$ configuration state functions calculations, show a large energy gap below the $4f^{13}5d(e_g)$ manifold, whose states are shifted by 22038±120 cm^{-1} with respect to the minimal RAS($4f$/5d6s-1e)SCF results. More important, the correlation energy corrections calculated at the subsequent RASPT2 step turn out to be very small: –721±571 cm^{-1}, as desirable for a second order perturbation.

Comparison of both RASPT2 calculations (labelled (1) and (2) in Table V) reveals that the PT2 corrections over the minimal RAS overestimate the differential correlation energy correction between the $4f^{14}$ ground state and the $4f^{13}5d(e_g)$ states, resulting in 14223±80 cm^{-1} too high $4f^{14} \rightarrow 4f^{13}5d(e_g)$ adiabatic transition energies. This constant error is basically due to the inaccuracy of the second order perturbation calculation of the differential radial correlation in the $4f$ shell. This is shown by computing the $^1A_{1g} \rightarrow 1^3T_{1u}$ adiabatic transition with the minimal RAS extended so as to include only the SD excitations to the second f-shell, which is accomplished with the so-called RAS($4f$-3h/5f/5d6s-1e)PT2 calculation for the $4f^{13}5d(e_g)$-1^3T_{1u} excited state and the RAS($4f$/5f-2e)PT2 calculation for

the ground state $4f^{14}$-$^1A_{1g}$ (in square parentheses in Table V), which gives a –12700 cm^{-1} shift, only +1500 cm^{-1} away from -14200 cm^{-1}. (Note the similarity with the second f-shell effect observed in the Yb^{2+} free ion in Table I: –13100 cm^{-1}.) The +1500 cm^{-1} difference should then be associated with the effects of double excitations to the $5d$ shell, with opposite sign than the double excitations to the $5f$ shell: although they stabilize the $4f^{14}$ ground configuration relative to the $4f^{13}$ one (so increasing the IP), they stabilize the $4f^{13}5d(e_g)$ states more strongly than the $4f^{14}$ ground state (so decreasing the $4f \rightarrow 5d$ transitions); nevertheless, their effect is small: <1500 cm^{-1}, in absolute value.

The RASPT2 values of the adiabatic IP ($4f^{14}\,1\,^1A_{1g} \rightarrow 4f^{13}\,1\,^2A_{2u}$) show a behavior similar to the $4f \rightarrow 5d$ transitions: The correlation energy correction calculated at the perturbational stage is very large when the reference is the minimal RAS (39300 cm^{-1}) and much smaller when the reference includes additional SD excitations to the $5d$, $5f$, and $6s$ shells (10900 cm^{-1}), so that the effect of the extensions to the RAS on the adiabatic ionization potential is –12000 cm^{-1}, hence, smaller than the –14200±80 cm^{-1} on the $4f^{13}5d(e_g)$ manifold.

Contrary to what happens with the inter-configurational electronic excitations, the equilibrium bond lengths and local totally symmetric vibrational frequencies in Table V show that the extensions of the minimal RAS have negligible effects on these structural properties.

Finally, we can compare the results of this work with those of Ref. 4, where the chosen RAS spaces were the single reference for the ground state and the CAS $4f5d6s$ for the excited states, and valence only AIMP embedded-cluster calculations were done using the valence basis set Yb[$6s5p6d4f1g$], Cl[$3s4p1d$], with the Sr[$5s1p$], Int[$5s$] extensions.[4] The CASPT2 $4f^{14} \rightarrow 4f^{13}5d(e_g)$ transition energies of Ref. 4 are +5233±480 cm^{-1} higher, in average, than the RAS($4f$-$3h$/$5d6s$/$5f$-$2e$)PT2 ones [cf. (3)–(2) in Table V]. These differences can be associated with: (a) the poor performance of the $(3g)/[1g]$ basis set used in the AIMP *vs.* the $(4g2h)[3g2h]$ ANO-RCC basis of the AE DKH calculations, (b) the lack of a second f-shell in the $4f$ and $4f5d6s$ CAS, and (c) other differences between the spin-orbit free AIMP and AE DKH calculations. Contributions (a) and (b) are large and partially cancell each other: Whereas (a) is close to –9000 cm^{-1}, as shown for the vertical IP of Yb^{2+} in gas phase and in $SrCl_2$ (Tables II and III), and by the comparison of the results of Ref. 4 with the minimal RASPT2 [cf. (3)–(1) in Table V: -8989±440 cm^{-1}], contribution (b) is about +12700 cm^{-1}, as discussed above. The remaining +1500 cm^{-1} discrepancy should be associated to other

differences between the spin-orbit free valence-only AIMP and all electron DKH calculations, such as the frozen-core approximation and the choices of relativistic Hamiltonians.

As mentioned in the Introduction, good agreement with the whole set of $4f \rightarrow 5d$ experimental transition energies was found in Ref. 4 after a constant –3500 cm^{-1} shift of the energies of the excited manifolds. The previous analyses suggest that a correction of the basis set limitations in the high angular momentum channels and a variational treatment of the SD excitations to the $5f$ shell (and $5d, 6s$ shells) in RAS($4f$-$3h$/$5d6s$/$5f$-$2e$)PT2 and RAS($4f$-$3h$/$5f$/$5d6s$-$1e$)PT2 calculations with an all electron DKH Hamiltonian would improve the agreements with experiments, leading to underestimations of 1700 cm^{-1} or even lower.

IV. CONCLUSIONS

In this work we have explored the effects of using a second f-shell in RASPT2 calculations of the lowest lying electronic excited states of Yb^{2+}-doped $SrCl_2$. We have performed exploratory RASPT2 calculations of the ionization potential of Yb^{2+} in gas phase and in $SrCl_2$ allowing for different levels of excitations (none, SD, and SDTQ) from the $4f$ shell to higher unoccupied shells and to a second f-shell in the RASSCF step, in order to decide upon the type of restricted active space to be used. Benchmark CCSD(T) calculations have been done. The effects of SD excitations to the second f-shell have been found to be very large and much larger than SD excitations to other unoccupied shells: they lower the IP of Yb^{2+} by 13100 cm^{-1} (6% of the J-averaged experimental value) in gas phase and by 13300 cm^{-1} in the $SrCl_2$ solid. These results give a measure of the importance of radial correlation in the $4f$ shell and of the error associated with its calculation using second order perturbation theory. Higher $4f$ to $5f$ excitations result in much smaller (in absolute value) increases in the IP (1300 cm^{-1}). Hence, the major effects of radial correlation in the $4f$ shell are captured at the SD excitation level. Comparisons of valence only AIMP and all electron DKH results of the IP of Yb^{2+} in gas phase and in $SrCl_2$ solid have revealed that the g basis set used in the valence only calculations is very poor and should be substituted by the high angular momentum ANO-RCC functions used with the all-electron Hamiltonian in order to obtain comparable results, which become very close to the averaged experimental value once the second f-shell effect is also included. The largest basis set error, detected

when the smallest $(3g)/[1g]$ AIMP and the largest $(4g2h)/[3g2h]$ ANO-RCC DKH basis set used are compared, results in an overestimation of the IP in both media close to 9000 cm^{-1}, which partially cancells the large lowering due to $4f$ radial correlation. The latter is shown to be quite basis set independent.

Multiconfigurational self-consistent field calculations including only the minimal $4f^{N-1}5d$ and $4f^{N-1}6s$ open-shell Hartree-Fock-like configurations in the restricted active space have been done on Yb^{2+}-doped $SrCl_2$ using all electron Douglas-Kroll-Hess Hamiltonian with the AIMP $SrCl_2$ embedding to serve as a reference for the study of electron correlation effects on the lowest electronic transition energies of the material. The results of this minimal RASSCF calculations show virtually no energy gap (5400 cm^{-1}) below the dense manifolds of excited states, in contrast with experimental evidence (25000 cm^{-1}; ∼29500 cm^{-1} without spin-orbit coupling), hence, the large experimental gap is associated with differential electron correlation. When subsequent multi-state second order perturbation theory (RASPT2) calculations are done, the energy gap and $4f^{14} \rightarrow 4f^{N-1}5d(e_g)$ transition energies are corrected by a 35599±439 cm^{-1} shift, in average, which is so large that the second order perturbation treatmet is unlikely to be valid. Alternatively, when SD excitations from the $4f$ to the $5d$, $6s$, and $5f$ shells are calculated variationally, the RASSCF energy gap and electronic transitions shift by 22038±120 cm^{-1} to higher energies, leaving much smaller correlation corrections (–721±571 cm^{-1}) to the second order perturbation RASPT2 step. Comparison of this extended RASPT2 with the minimal RASPT2 transition energies shows a quite constant –14223±80 cm^{-1} shift, the major contribution to which is associated with variational calculation of the SD excitations to the second f shell: –12700 cm^{-1}. This effect is very close to that observed for the IP of the free and doped Yb^{2+} ion.

The results of this work allow to understand the overall +3500 cm^{-1} overestimation of the theoretical *vs.* experimental absorption bands of $SrCl_2$:Yb^{2+} obtained in previous work (Refs. 4 and 5) as a compensation of two errors: (a) the lack of a second f-shell in the active space (+12700 cm^{-1}) and (b) the poor performance of the $(3g)/[1g]$ basis set used (–9000 cm^{-1}).

Acknowledgments

This work was partly supported by a grant from Ministerio de Economía y Competitividad, Spain (Dirección General de Investigación y Gestión del Plan Nacional de I+D+i, MAT2011-24586).

---

[1] T. S. Piper, J. P. Brown, and D. S. McClure, J. Chem. Phys. **46**, 1353 (1967).

[2] H. Witzke, D. S. McClure, and B. Mitchell, in *Luminescence of Crystals, Molecules, and Solutions*, edited by F. E. Williams (Plenum, New York, 1973), p. 598.

[3] Z. Pan, C. Duan, and P. A. Tanner, Phys. Rev. B **77**, 085114 (2008).

[4] G. Sánchez-Sanz, L. Seijo, and Z. Barandiarán, J. Chem. Phys. **133**, 114509 (2010).

[5] G. Sánchez-Sanz, L. Seijo, and Z. Barandiarán, J. Chem. Phys. **133**, 114506 (2010).

[6] F. Ruipérez, Z. Barandiarán, and L. Seijo, J. Chem. Phys. **127**, 144712 (2007).

[7] B. O. Roos, P. R. Taylor, and P. E. M. Siegbahn, Chem. Phys. **48**, 157 (1980); P. E. M. Siegbahn, A. Heiberg, J. Almlöf, and B. O. Roos, J. Chem. Phys. **74**, 2384 (1981); P. Siegbahn, A. Heiberg, B. Roos, and B. Levy, Phys. Scr. **21**, 323 (1980).

[8] K. Andersson, P.-Å. Malmqvist, B. O. Roos, A. J. Sadlej, and K. Wolinski, J. Phys. Chem. **94**, 5483 (1990).

[9] K. Andersson, P.-Å. Malmqvist and B. O. Roos, J. Chem. Phys. **96**, 1218 (1992).

[10] A. Zaitsevskii and J. P. Malrieu, Chem. Phys. Lett. **233**, 597 (1995).

[11] J. Finley, P.-Å. Malmqvist, B. O. Roos and L. Serrano-Andrés, Chem. Phys. Lett. **288**, 299 (1998).

[12] C. Froese-Fischer, J. Phys. B **10**, 1241 (1977).

[13] T. H. Dunning, Jr., B. H. Botch and J. F. Harrison, J. Chem. Phys. **72**, 3419 (1980).

[14] K. Pierloot, in *Advances in Chemical Physics: New Methods in Computational Quantum Mechanics*, edited by T. R. Cundari (Deker, New York, 2001).

[15] K. Pierloot and S. Vancoillie, J. Chem. Phys. **125**, 124303 (2006).

[16] P.-Å. Malmqvist, K. Pierloot, A. R. Moughal Shahi, C. J. Cramer and L. Gagliardi, J. Chem. Phys. **128**, 204109 (2008).

[17] V. Sauri, L. Serrano-Andrés, A. R. Mougal Shahi, L. Gagliardi, S. Vancoillie and K. Pierloot,

J. Chem. Theory Comput. **7**, 153 (2011).

[18] B. Ordejón, L. Seijo, and Z. Barandiarán, J. Chem. Phys. **126**, 194712 (2007).

[19] Z. Barandiarán, L. Seijo, and A. Wojtowicz, unpublished.

[20] Z. Barandiarán, L. Seijo, and S. Huzinaga, J. Chem. Phys. **93**, 5843 (1990); Z. Barandiarán and L. Seijo, Can. J. Chem. **70**, 409 (1992); J. Chem. Phys. **101**, 4049 (1994).

[21] M. Douglas and N. M. Kroll, Ann. Phys. (N.Y.) **82**, 89 (1974).

[22] B. A. Hess, Phys. Rev. A **33**, 3742 (1986).

[23] B. O. Roos, R. Lindh, P.-Å. Malmqvist, V. Veryazoz, P.-O. Widmark, and A. C. Borin, J. Phys. Chem. A **112**, 11431 (2008).

[24] J. Olsen, B. O. Roos, P. Jørgensen, and J. A. Jensen, J. Chem. Phys. **89**, 2185 (1988).

[25] P.-A. Malmqvist, A. Rendell, and B. O. Roos, J. Phys. Chem. **94**, 5477 (1990).

[26] G. Ghigo, B. O. Roos, and P.-Å. Malmqvist, Chem. Phys. Lett. **396**, 142 (2004).

[27] V. Kaufman and J. Sugar, J. Opt. Soc. Amer. **66**, 1019 (1976).

[28] W. C. Martin, R. Zalubas, and L. Hagan, *Atomic Energy Levels - The Rare Earth Elements*, Nat. Stand. Ref. Data Ser., Natl. Bur. Stand. No. 60 (U. S. GPO, Washington, D. C., 1978).

[29] V. A. Dzuba and G. F. Gribakin, J. Phys. B: At. Mol. Opt. Phys. **31**, L483 (1998).

[30] L. Seijo, Z. Barandiarán, and B. Ordejón, Mol. Phys. **101**, 73 (2003).

[31] L. Seijo, Z. Barandiarán, and E. Harguindey, J. Chem. Phys. **114**, 118 (2001).

[32] K. Raghavachari, G. W. Trucks, J. A. Pople and M. Head-Gordon, Chem. Phys. Lett. **157**, 479 (1989).

[33] J. D. Watts, J. Gauss, and R. J. Bartlett, J. Chem. Phys. **98**, 8718 (1983).

[34] P. Neogrády, M. Urban, and I. Hubač, J. Chem. Phys. **97**, 5074 (1992).

[35] P. Neogrády, M. Urban, and I. Hubač, J. Chem. Phys. **100**, 3706 (1994).

[36] R. W. G. Wyckoff, *Crystal Structures*, vol. 1, 2nd. edn. (Interscience Publishers, 1982).

[37] Z. Barandiarán and L. Seijo, J. Chem. Phys. **89**, 5739 (1988).

[38] L. Seijo and Z. Barandiarán, in *Computational Chemistry: Reviews of Current Trends*, edited by J. Leszczyński (World Scientific, Singapore, 1999), vol. 4, p. 55.

[39] A. Gellé and M. B. Lepetit, J. Chem. Phys. **128**, 244716 (2008).

[40] G. Karlström, R. Lindh, P. A. Malmqvist, B. O. Roos, U. Ryde, V. Veryazov, P. O. Widmark, M. Cossi, B. Schimmelpfennig, P. Neograd y, and L. Seijo, Comput. Mater. Sci. **28**, 22 (2003).

[41] Detailed core and embedding AIMP data libraries in electronic format are available from

the authors upon request or directly at the address http://www.uam.es/quimica/aimp/Data/-AIMPLibs.html. See also Ref. 40.

[42] L. Seijo and Z. Barandiarán, J. Chem. Phys. **118**, 5335 (2003).

[43] X. Cao and M. Dolg, Chem. Phys. Lett. **349**, 489 (2001).

[44] R. McWeeny, *Methods of molecular quantum mechanics* (Academic Press, London, 1989), 2nd ed.

[45] See supplementary material at [URL] for details and results of the study of convergence of extensions of the Yb and Cl basis set with Sr and Interstice basis functions.

TABLE I: Values of the ionization potential (IP) of Yb^{2+} calculated using the core [Kr] AIMP Hamiltonian, Yb [$6s5p6d4f1g$] basis set, and the RASPT2, CCSD, and CCSD(T) methods to correlate 22(Yb^{2+})/21(Yb^{3+}) valence electrons. RASSCF values are also given. Orbitals included in the RAS2 and RAS3 subspaces and maximum number of electrons allowed in the latter are indicated. See text for details. Differences with CCSD(T) ($\Delta_{CCSD(T)}$) and averaged experimental (Δ_{exp}) values are given. Energies in cm^{-1}. D_{2h} symmetry has been used.

Calc.			RASSCF					RASPT2		
	RAS2	RAS3	IP	ncfg [1]		ref. weight [2]		IP	$\Delta_{CCSD(T)}$	Δ_{exp} [3]
				Yb^{2+} $^1S(^1A_g)$	Yb^{3+} $^2F(^2A_u)$	Yb^{2+} $^1S(^1A_g)$	Yb^{3+} $^2F(^2A_u)$			
						without double f-shell				
1	$4f$	none	168097	1	1	0.87	0.90	209394	11361	2947
2	$4f5d6s$	none	171492	92708	161039	0.88	0.91	211710	13676	5263
		2e max.								
3	$4f$	$5d$	171338	172	784	0.88	0.91	211660	13626	5213
4	$4f$	$5d6s$	171376	244	1138	0.88	0.91	211678	13645	5231
		4e max.								
5	$4f$	$5d$	171452	5098	15232	0.88	0.91	211695	13662	5248
6	$4f$	$5d6s$	171492	11143	33655	0.88	0.91	211711	13677	5264
						with double f-shell				
		2e max.								
7	$4f$	$5f$	182279	339	1635	0.91	0.93	196287	-1747	-10160
8	$4f$	$5d5f$	184670	510	2418	0.92	0.94	197640	-393	-8807
9	$4f$	$5d5f6s$	184697	582	2772	0.92	0.94	197636	-397	-8811
10	$4f$	$5d5f6s6p$	184416	912	4446	0.92	0.94	197601	-432	-8846
		4e max.								
11	$4f$	$5f$	184041	24865	78745	0.91	0.94	197569	-465	-8878
12	$4f$	$5d5f$	187654	110674	349702	0.92	0.94	200414	2381	-6033
13	$4f$	$5d5f6s$	187684	153013	484177	0.92	0.94	200471	2437	-5976
14	$4f$	$5d5f6s6p$	187463	352437	1115931	0.92	0.94	200496	2462	-5951
								Coupled cluster energies		
							CCSD	194676	-3358	-11771
							CCSD(T)	198034	0	-8413

[1] Number of configurations generated at the RASSCF level for the ^1A_g and ^2A_u D_{2h} components of Yb^{2+} ^1S and Yb^{3+} ^2F states, respectively.

[2] Weight of the ^1A_g and ^2A_u RASSCF reference in the RASPT2 wave functions, respectively.

[3] Experimental values and their average (Refs. 27, 28): $4f^{14}$ $0(^1S)\rightarrow 4f^{13}$ $7/2(^2F)$: 202070; $4f^{14}$ $0(^1S)\rightarrow 4f^{13}$ $5/2(^2F)$: 212285; $4f^{14}$ $0(^1S)\rightarrow 4f^{13}$ ave(^2F): 206447 cm^{-1}.

TABLE II: Basis set effects and reference space effects on valence-only AIMP and all-electron DKH calculations of the Yb^{2+} ionization potential using the RASPT2 method to correlate 22(Yb^{2+})/21(Yb^{3+}) valence electrons. Differences relative to corresponding CCSD(T) calculations, ($\Delta_{CCSD(T)}$) and averaged experimental value (Δ_{exp}) are also given. All numbers in cm^{-1}. See footnotes of Table I for experimental values. Calculations have been done using C_i point symmetry.

	RASPT2 reference space [1]									
	$4f5d6s$			$4f$			$4f/5d5f6s$-$2e$			
basis set	IP	Δ_{exp}	$\Delta_{CCSD(T)}$	IP	Δ_{exp}	$\Delta_{CCSD(T)}$	IP	Δ_{exp}	$\Delta_{CCSD(T)}$	
	1			2			3			3 – 2
AIMP with $(3g)/[ng]$ functions from maximum radial overlap to the $4f$ atomic orbital										
$[6s5p6d4f1g]$	211710	5263	13676	209381	2934	11347	197623	-8824	-411	-11758
$[6s5p6d4f2g]$	216312	9865		214373	7926		202470	-3977		-11904
$[6s5p6d4f3g]$	217226	10779		215327	8880		203353	-3094		-11975
AIMP with ng functions from ANO-RCC basis set										
$[6s5p6d4f1g]$				214451	8004		202614	-3833		-11838
$[6s5p6d4f2g]$				216047	9600		204088	-2359		-11959
$[6s5p6d4f3g]$				216328	9881		204422	-2025		-11906
AE DKH with ANO-RCC basis set										
$[9s8p5d4f1g]$				215941	9494		203640	-2807		-12301
$[9s8p5d4f2g]$				217674	11227		205417	-1030		-12256
$[9s8p5d4f3g]$				217661	11214	13475	205430	-1017	1244	-12231
$[9s8p5d4f3g2h]$				218468	12021	13401	206265	-182	1198	-12203

[1] The maximum number of electrons allowed in RAS3 (ne) is indicated.

TABLE III: All electron DKH vertical ionization potential of $(YbCl_8)^{6-}$ embedded in $SrCl_2$, calculated at R(Yb–Cl)=2.95Å. The RASPT2 and CCSD(T) methods are used to correlate 86 (L64M22) and 85 (L64M21) valence electrons of the Yb^{2+} $4f^{14}$-$^1A_{1g}$ and Yb^{3+} $4f^{13}$-$^2A_{2u}$ states, respectively. Basis set truncation effects are shown in parentheses. Valence-only AIMP results with a smaller valence basis set are also included. All numbers are given in cm^{-1}.

basis set		RASPT2 reference space[1]				CCSD(T)		$\Delta_{CCSD(T)}$	
Yb	Cl	$4f$		$4f/5d5f$-2e					
		1		2		3		1–3	2–3
$[9s8p5d4f3g2h]$	$[6s5p3d2f]$	58075	(0)	46061	(0)	43941	(0)	14135	2120
	$[6s5p3d]$	57980	(-95)	45973	(-88)	43566	(-375)	14414	2407
	$[6s5p2d]$	57613	(-462)	45600	(-461)	43155	(-786)	14458	2445
	$[6s5p1d]$	56797	(-1278)	44792	(-1269)	42251	(-1690)	14546	2541
$[9s8p5d4f3g]$	$[6s5p3d2f]$	57401	(-674)	45359	(-702)	43254	(-687)	14147	2106
AIMP									
$[6s5p6d4f1g]$	$[3s4p1d]$	49167	(-8908)	37410	(-8651)	37022	(-6919)	12145	388

[1] The maximum number of electrons allowed in RAS3 (ne) is indicated.

TABLE IV: Effects of extensions of the $(YbCl_8)^{6-}$ cluster and Yb[9s8p5d4f3g2h] Cl[6s5p3d] molecular basis set on the Yb–Cl bond lengths, R_e, totally symmetric vibrational frequencies, $\bar{\nu}_{a_{1g}}$, and adiabatic ionization potential, IP, of $SrCl_2$:Yb^{2+} calculated using the RASSCF, RASPT2, and CCSD(T) methods to correlate 86 (L64M22) and 85 (L64M21) valence electrons of the Yb^{2+} $4f^{14}$-$^1A_{1g}$ and Yb^{3+} $4f^{13}$-$^2A_{2u}$ states, respectively. The maximum number of electrons (ne) allowed in the RAS3 subspace is indicated. See text for details. Distances are given in Å, energies in cm^{-1}. Int stands for (1/2,0,0) interstitial sites.

		RAS 4f		RAS 4f/5d5f-2e				
Property		RASSCF	RASPT2	RASSCF	RASPT2	CCSD(T)	$\Delta_{CCSD(T)}$	
			1		2	3	1 – 3	2 – 3
A. $(YbCl_8)^{6-}$ Yb[9s8p5d4f3g2h] Cl[6s5p3d]								
$^1A_{1g}$	R_e	2.966	2.848	2.963	2.855			
	$\bar{\nu}_{a_{1g}}$	204	214	205	214			
$^2A_{2u}$	R_e	2.804	2.710	2.803	2.715			
	$\bar{\nu}_{a_{1g}}$	255	265	255	265			
	IP	7025	46347	23416	34614			
B. $(YbCl_8Sr_{12})^{18+}$ Yb[9s8p5d4f3g2h] Cl[6s5p3d] Sr[5s1p][1] Int[5s][1]								
$^1A_{1g}$	R_e	3.056	2.927	3.054	2.935	2.959	–0.032	–0.024
	$\bar{\nu}_{a_{1g}}$	182	192	182	192	196	–4	–4
$^2A_{2u}$	R_e	2.867	2.765	2.865	2.770	2.791	–0.026	–0.021
	$\bar{\nu}_{a_{1g}}$	233	242	233	242	240	2	2
	IP	17390	56396	33753	44726	43531	12865	1195
C. $(YbCl_8Sr_{12})^{18+}$ Yb[9s8p5d4f3g2h] Cl[6s5p3d] Sr[5s4p][2] Int[4s][2]								
$^1A_{1g}$	R_e	3.101	2.969	3.099	2.977			
	$\bar{\nu}_{a_{1g}}$	169	179	170	180			
$^2A_{2u}$	R_e	2.892	2.787	2.890	2.793			
	$\bar{\nu}_{a_{1g}}$	223	232	223	233			
	IP	21461	60766	37850	48771			

[1] Sr and interstice bases from Ref. 4.

[2] This work: Sr and interstice bases resulting from a basis set convergence study (Ref. 45).

TABLE V: Spectroscopic constants of the ground and $4f^{13}5d(e_g)$ excited states of Yb^{2+}, and $4f^{13}$-$^2A_{2u}$ state of Yb^{3+}-doped $SrCl_2$. 86(Yb^{2+}) and 85(Yb^{3+}) electrons are correlated using the multi-state RASPT2 method. Yb–Cl bond distances, R_e, in Å; totally symmetric vibrational frequencies, $\bar{\nu}_{a_{1g}}$, in cm^{-1}; and minimum-to-minimum energy differences, T_e, relative to the $4f^{14}$–1^1A_{1g} ground state, in cm^{-1}.

	RASPT2 [1]			RASPT2 – RASSCF			
state $(ncfg)^2$	R_e	$\bar{\nu}_{a_{1g}}$	T_e	R_e	$\bar{\nu}_{a_{1g}}$	T_e	T_e
		(1) $4f/5d6s$-$1e$					
$1\ ^1A_{1g}$	2.969	179	0	-0.132	10	0	
$\langle 4f^{13}5d(e_g)\rangle$	2.904±0.006	181±2		-0.153±0.007	7±2	35539±439	
$1\ ^3T_{1u}$ (11)	2.915	180	41682	-0.147	7	36255	
$1\ ^3T_{2u}$	2.908	180	44220	-0.148	6	35901	
$1\ ^1T_{2u}$ (11)	2.905	181	44793	-0.150	6	35395	
$2\ ^3T_{1u}$	2.910	179	45057	-0.148	6	35654	
$1\ ^1E_u$ (9)	2.904	180	45306	-0.150	6	35508	
$1\ ^3E_u$ (9)	2.907	179	45271	-0.150	6	36157	
$1\ ^1T_{1u}$	2.894	181	45850	-0.167	9	34912	
$2\ ^1T_{1u}$	2.894	186	46853	-0.165	12	35497	
$2\ ^3T_{2u}$	2.904	179	46947	-0.149	4	35106	
$2\ ^1T_{2u}$	2.898	185	47438	-0.154	10	35008	
$1\ ^2A_{2u}$	2.787	232	60766	-0.105	9	39305	
		(2) $4f$-$3h/5d6s/5f$-$2e$ [3]					(2) [3] – (1)
$1\ ^1A_{1g}$	2.977	180	0	-0.122	10	0	0
$\langle 4f^{13}5d(e_g)\rangle$	2.909±0.003	180±2		-0.148±0.002	7±2	-721±571	-14223±80
$1\ ^3T_{1u}$ (19492) (16183)	2.915 [2.917]	180 [176]	27581 [28949]	-0.147	7	339	-14101 [-12733]
$1\ ^3T_{2u}$	2.908	180	30068	-0.148	6	-255	-14152
$1\ ^1T_{2u}$ (12003)	2.906	184	30474	-0.148	9	-842	-14319
$2\ ^3T_{1u}$	2.911	181	30950	-0.147	8	-494	-14107
$1\ ^1E_u$ (11969)	2.911	180	31060	-0.143	6	-761	-14246
$1\ ^3E_u$ (19476)	2.911	179	31076	-0.146	6	-146	-14195
$1\ ^1T_{1u}$	2.912	176	31539	-0.150	4	-1395	-14311
$2\ ^1T_{1u}$	2.907	177	32616	-0.152	4	-761	-14237
$2\ ^3T_{2u}$	2.906	182	32723	-0.146	7	-1370	-14224
$2\ ^1T_{2u}$	2.903	184	33104	-0.148	9	-1526	-14334

$1\ ^2A_{2u}$	2.793	233	48771	-0.097	10	10921	-11995
		(3) $4f5d6s$ [4]					(3) [4] – (2)
$1\ ^1A_{1g}$	2.954	184	0	-0.122	10	0	0
$\langle 4f^{13}5d(e_g)\rangle$	2.899±0.003	203±5		-0.142±0.004	26±4	29616±599	5233 ±480
							(3) [4] – (1)
$\langle 4f^{13}5d(e_g)\rangle$							-8989±440

[1] The restricted active space used in the RASSCF calculations is indicated. The maximum number of holes in RAS1 (-nh) and of electrons in RAS3 (-ne) are indicated.

[2] Number of configurations generated for the $^{3,1}A_u$ and $^{3,1}B_{1u}$ D_{2h} symmetry blocks are given in parenthesis for the lowest O_h state of each block. Manifold averages and mean square deviations of the individual values are labeled $\langle 4f^{13}5d(e_g)\rangle$.

[3] The $4f/5f$-$2e$ and $4f$-$3h/5f/5d6s$-$1e$ restricted active spaces have been used for the calculation of the 1^1A_{1g} and 1^3T_{1u} states, respectively, to compute the $1^1A_{1g}\rightarrow 1^3T_{1u}$ transition energy; results are shown in brackets. See text for details.

[4] From Ref. 4: Multi-state CASPT2 results using the $4f5d6s$ CAS.

FIG. 1: Breathing mode potential energy curves of the states of the $SrCl_2$ $(YbCl_8Sr_{12})^{18+}$/ $(YbCl_8Sr_{12})^{19+}$ embedded clusters, with dominant configurational character $4f^{14}$ (black line and bullets), $4f^{13}5d(e_g)$ (red lines and bullets), and $4f^{13}$ (violet line and filled squares), in increasing energy order. The results have been obtained using the scalar relativistic all electron Douglas-Kroll-Hess Hamiltonian with the $SrCl_2$ Ab Initio Model Potetial embedding. Graphs on the left: RASSCF results; the RAS is indicated. Graphs on the right: multi-state RASPT2 results; $86(Yb^{2+})$ or $85(Yb^{3+})$ electrons are correlated. See text for details.

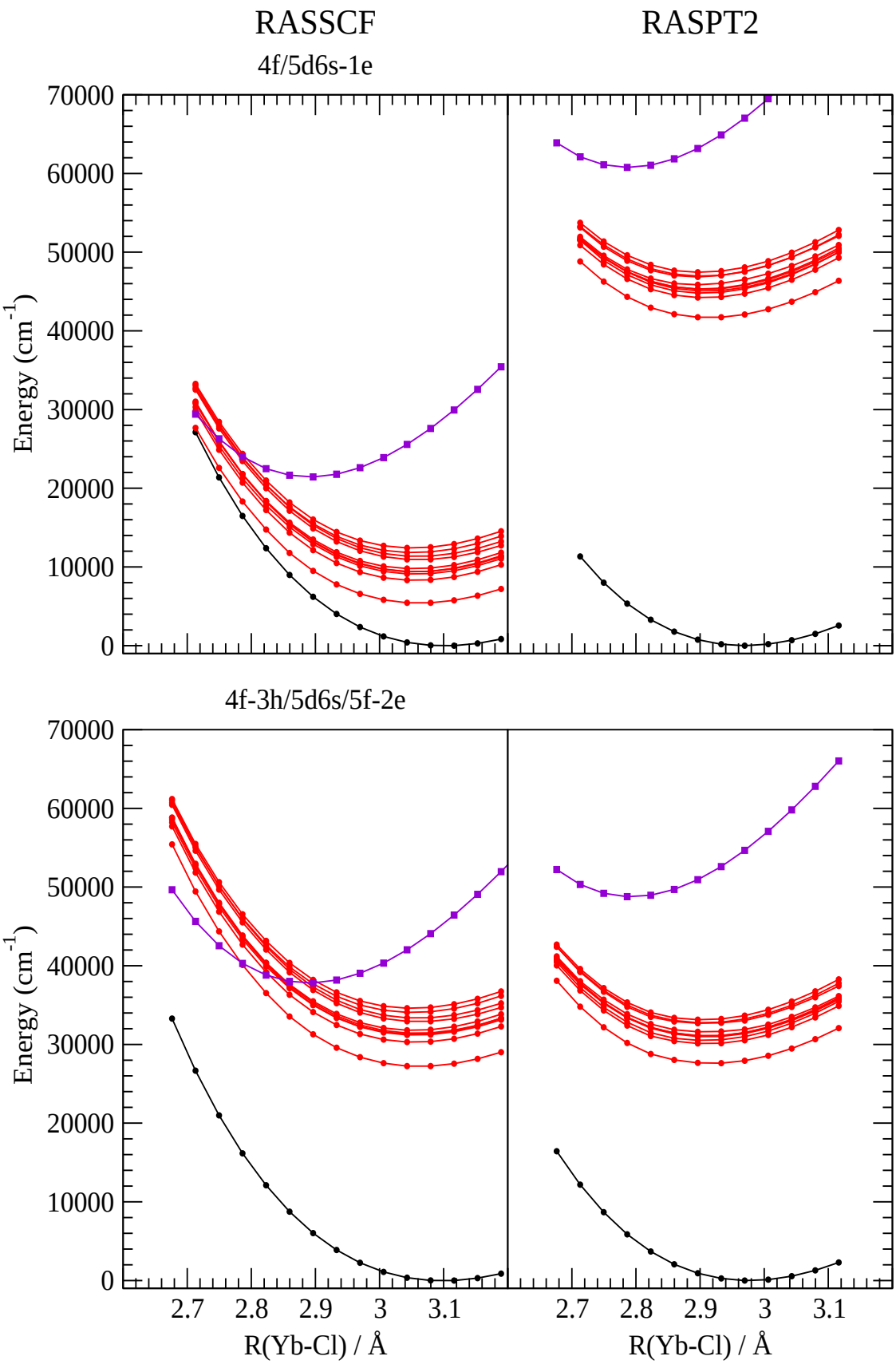

Figure 1. Barandiarán *et al.*, Journal of Chemical Physics